Multivalent Noncovalent Interfacing and Cross-Linking of Supramolecular Tubes

Fangyuan Xiu, Anamarija Knežević, Supaporn Kwangmettatam, Daniele Di Iorio, Jurriaan Huskens, and Tibor Kudernac*

Natural supramolecular filaments have the ability to cross-link with each other and to interface with the cellular membrane via biomolecular noncovalent interactions. This behavior allows them to form complex networks within as well as outside the cell, i.e., the cytoskeleton and the extracellular matrix, respectively. The potential of artificial supramolecular polymers to interact through specific noncovalent interactions has so far only seen limited exploration due to the dynamic nature of supramolecular interactions. Here, a system of synthetic supramolecular tubes that cross-link forming supramolecular networks, and at the same time bind to biomimetic surfaces by the aid of noncovalent streptavidin–biotin linkages, is demonstrated. The architecture of the networks can be engineered by controlling the density of the biotin moiety at the exterior of the tubes as well as by the concentration of the streptavidin. The presented strategy provides a pathway for designing adjustable artificial supramolecular superstructures, which can potentially yield more complex biomimetic adaptive materials.

1. Introduction

Function and behavior of industrial and biomolecular materials that are constituted by covalent and supramolecular polymer networks critically depend not only on the molecular structure and organization of the monomers and the length of

F. Xiu, A. Knežević, S. Kwangmettatam, D. Di Iorio, J. Huskens, T. Kudernac
Molecular Nanofabrication Group
MESA+ Institute for Nanotechnology
University of Twente
PO Box 207, Enschede 7500 AE, The Netherlands
E-mail: t.kudernac@rug.nl
A. Knežević
Division of Organic Chemistry and Biochemistry
Ruđer Bošković Institute
Bijenička cesta 54, Zagreb 10000, Croatia
T. Kudernac
Faculty of Science and Engineering
Molecular Inorganic Chemistry – Stratingh Institute for Chemistry
Nijenborgh 4, Groningen 9747 AG, The Netherlands

the individual fibers, but also on the way how they interact with each other and with their surroundings.[1,2] For instance, in organisms, the fine mechanical properties of the cellular actin filament system are determined by the cross-linking density and their dynamics,[3] and actin networks can cross-link via microtubule-associated proteins with stiff microtubules,[4] yielding a complex network that helps in resisting shear stresses.[5] The extracellular matrix is also a network of cross-linked fibers that are further tethered to the cell membrane through associated proteins by single or multivalent interactions.[6,7] These provide structural support for the cell[8] and tissue integrity under growth,[9] enabling remodeling of the tissue under ever changing environmental conditions. Dynamic cross-linking of the fibers and their engineered binding with the surroundings is thus a critical parameter for proper functioning.

Controlled cross-linking of covalent polymeric fibers has been widely exploited to prepare designed polymer materials and hydrogels.[10,11] Numerous strategies have been developed for controlled interfacing of these polymer networks with solid substrates via specific interactions including on-surface growth of polymer networks.[12,13] These avenues have been explored in supramolecular polymer systems to much lesser extent, primarily relying on poorly controlled and nonspecific interactions between supramolecular fibers.[14] Recently reported chemically cross-linked supramolecular fibers yielding strain-stiffening, self-healing hydrogels demonstrate their potential as dynamic new materials.[15] The ability to respond to changes or self-heal arises from the intrinsically reversible exchanges between monomer and (supramolecular) polymer states.[16] Pioneering work by Stupp and co-workers on peptide–DNA conjugates' cross-linking of supramolecular fibers provides a tantalizing hint of the potential of controlled cross-linking for the generation of reversible highly organized synthetic superstructures.[17] Progress in the field of interfacing supramolecular polymers is, however, hampered by the dynamic nature of the architecture itself. Reversible noncovalent interactions that hold supramolecular structures together enable recruitment of binding groups or removal of the active binder from the structure.[18] Furthermore, supramolecular aggregates containing biotin as guests have been shown to selectively disassemble upon interaction with complementary avidin as complementary multivalent host unit.[19] Recently, the crucial role of multivalent

ADVANCED
SCIENCE NEWS
www.advancedsciencenews.com
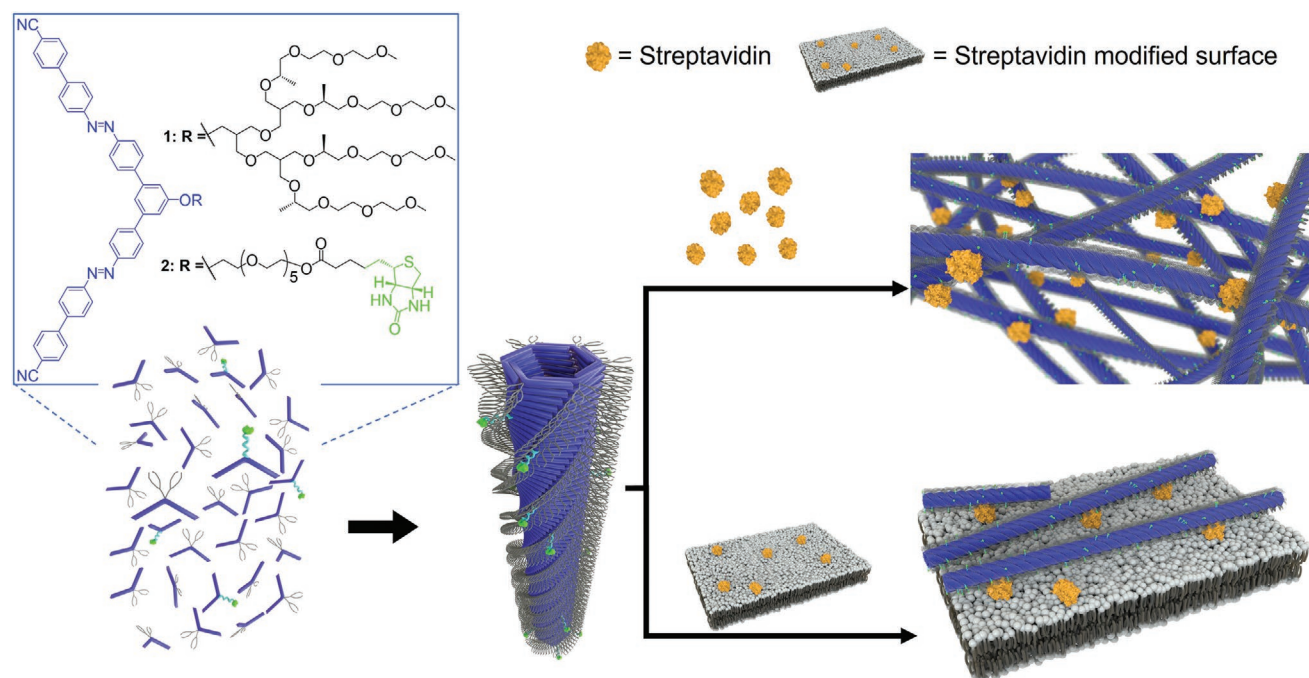
ADVANCED
MATERIALS
www.advmat.de

Figure 1. SAv-mediated cross-linking and surface binding of supramolecular polymers formed by coassembly of compounds **1** and **2**.

binding was demonstrated in anchoring functional copolymers on the surface of human erythrocytes via a dynamic covalent chemistry approach.[20] This work on the cell–supramolecular polymer interactions illustrates that our insight into how these dynamic structures react and adapt to interfacing is still quite limited at this point.

Here, we present an entirely noncovalent complex network system formed by synthetic supramolecular polymers that interact with each other and with other objects in a controlled and specific way. The supramolecular polymer, generated by coassembly of structurally related biotinylated building blocks with chiral aromatic building blocks, is formed in water which provides a life-like environment compatible with already developed platforms for natural and biomimetic systems. Biotin moieties incorporated within supramolecular polymer systems enable the cross-linking of polymers upon addition of streptavidin (SAv), as well as interfacing these polymers to SAv-modified cell-membrane-mimicking surfaces. The cross-linking network is tunable by the ratios of both the biotinylated building blocks and SAv, while effective binding to a SAv-modified surface can be tuned by varying the fraction of biotin moieties within the supramolecular tubes. The resulting architecture of the network can be tuned by selecting specific concentration of the individual (bio)molecular components. Ultimately, this network tuning should prove valuable in engineering mechanical properties of the presented materials. Finally, the complex artificial system is constructed based solely on supramolecular interactions, resembling natural systems in which supramolecular interactions play a crucial role to achieve the desired functions, e.g., porosity, stiffness, plasticity, etc. This artificial system can be considered a simplified model of natural cellular architectures formed from individual fibers, since it exhibits the formation of a complex network of 1D supramolecular

polymers, and it can be bound to the supported lipid bilayer, i.e., a cell membrane model.

2. Results and Discussion

2.1. Design of Supramolecular Polymer System

Our strategy for the construction of stable supramolecular networks is based on the modular nature of supramolecular polymers (**Figure 1**). We designed the amphiphilic building blocks **1** and **2** that feature the same hydrophobic V-shaped aromatic part, and a hydrophilic oligo(ethylene glycol) unit. Previously, we have demonstrated that compound **1** in water assembles into stiff tubes with slow exchange rates between monomers in the solution and in the self-assembled state.[21] Compound **2** bears a biotin moiety as the linker unit, connected with an azobenzene-based moiety through a sufficiently long oligo(ethylene glycol) chain. In water, **1** and **2** coassemble due to the same hydrophobic core, and driven by hydrophobic effects, π–π interactions and shape recognition[22] form a supramolecular copolymer. The resulting supramolecular tube has both the ability to form a complex cross-linking network upon addition of SAv that has four binding sites for biotin, as well as to be firmly bound to SAv-modified surfaces (Figure 1). Interaction between biotin and SAv that can be codissolved in the solution provides highly specific and strong interaction[23] which has already been employed for the analysis of interaction of biotinylated amphiphilic peptides with avidin[24] and for templating protein assembly by supramolecular fibers.[25] Furthermore, SAv-coated surfaces and interfacing platforms have been previously reported,[26] while SAv itself has high stability when complexed with biotins.[27,28]
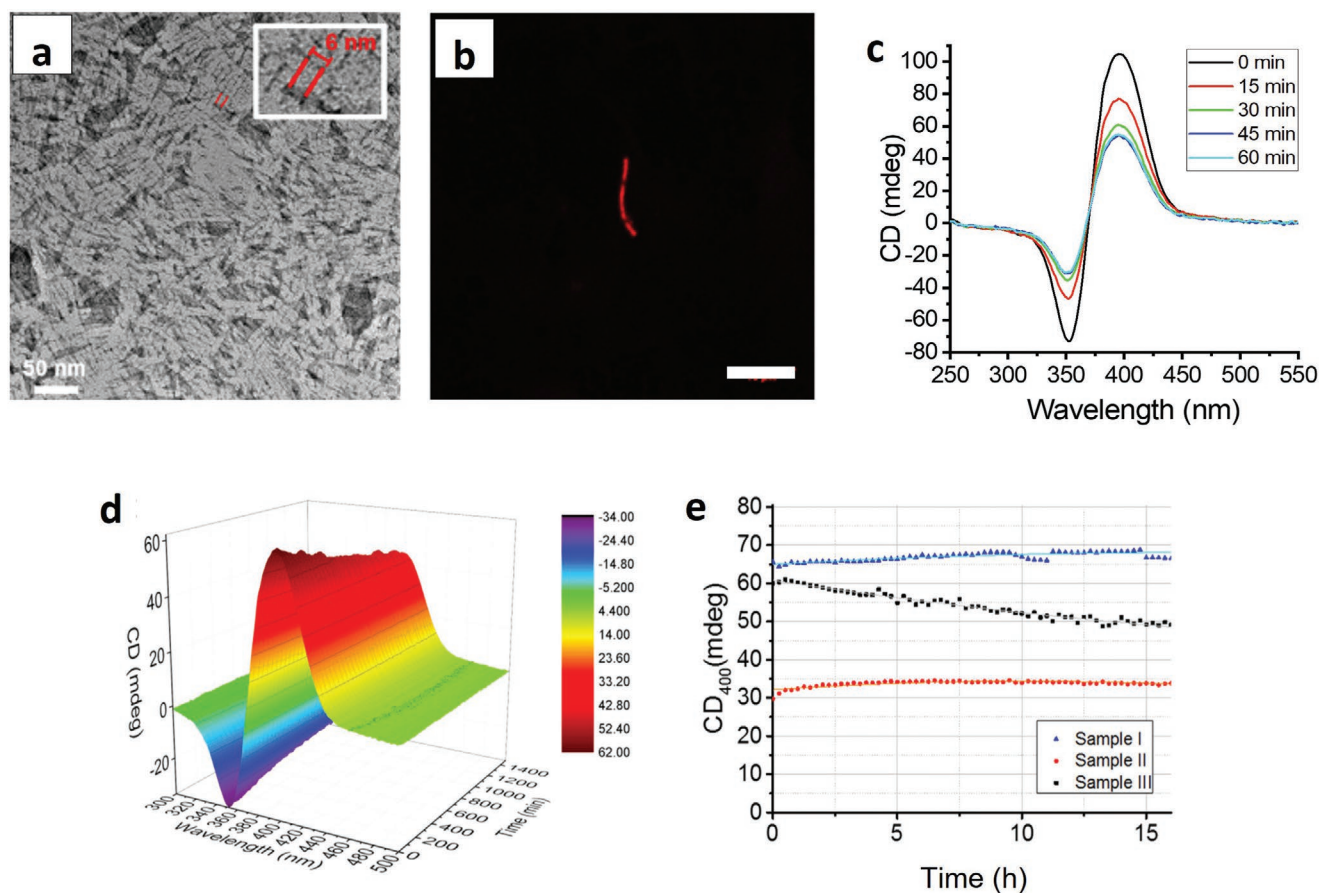
**ADVANCED
SCIENCE NEWS**

www.advancedsciencenews.com

**ADVANCED
MATERIALS**

www.advmat.de

Figure 2. Morphology and coassembly of **1**–**2** tubes. a) TEM images and b) CLSM images of the supramolecular **1**–**2** tubes (50:1) incorporating Nile red. Scale bar: 10 µm. c) CD spectra of 100×10^{-6} M solution of **1**–**2** tubes (50:1) upon irradiation ($\lambda = 365$ nm). d) CD spectra of the mixture of preassembled solutions of **1** (10×10^{-6} M) and **2** (10×10^{-6} M) in 5% MeCN/water in 1:1 volume ratio with the final concentration of each component of 5×10^{-6} M (sample III) observed during 16 h. e) Plot of CD intensities at $\lambda = 400$ nm versus time of sample I (5×10^{-6} M solution of **1**), sample II (solution of **1** and **2** mixed prior to the formation of the self-assembled structures with 5×10^{-6} M concentration of each molecular component), and sample III.

2.2. Coassembly of 1 and 2 into a Bicomponent Supramolecular Polymer

Compound **2** was successfully synthesized using the same strategy as for the synthesis of **1** (Figure S1, Supporting Information). Transmission electron microscopy (TEM) images of a dried solution of **2** revealed the formation of disordered ribbons (Figure S2, Supporting Information), in contrast to the elongated tubular architectures observed in TEM images of **1** (Figure S3, Supporting Information). This structural difference may be the result of reduced hydrophilic volume in the structure of **2** with only one oligo ethylene chain, as observed previously for other bent-shaped amphiphiles with varying hydrophobic–hydrophilic volume ratios.[26] Solution of **1** in water above 1×10^{-6} M, which is the critical aggregation concentration (CAC), shows a pronounced circular dichroism (CD) signal due to the formation of chiral tubes with preferential helicity.[21] By contrast, the chirality of the stereogenic centers in the biotin moiety of **2** is not transmitted to the supramolecular structure as no significant CD signal was observed for the solution of **2** in MeCN, as well as in water (Figure S2, Supporting Information).

Incorporation of a small amount of **2** into the solution of **1** had a negligible effect on the tubular architecture of **1**, given the identical hydrophobic aromatic core. TEM images confirmed that morphology of the tubes formed by the mixture of **1** and **2** (50:1 molar ratio) (**Figure 2**a) was identical to the tubes formed exclusively by **1**, with the same 6 nm diameter of the tubes. The length and the size distribution of the tubes formed by **1** and **2** could not be established but given the small proportion of **2** and the apparent similarity of the microscopy images, it is expected to be similar to the previously reported tubes made of **1**.[21] Rod-like structures were observed upon drying of solution of **1**–**2** tubes (50:1 molar ratio) stained by Nile red on the glass substrate (Figure 2b) using confocal laser-scanning microscope (CLSM). Similar morphology was previously observed for water-soluble benzene-1,3,5-tricarboxamide-based supramolecular polymers.[27] These elongated structures are likely aggregated bundles of tubes formed during evaporation of the solvent in an open chamber. There is no difference between the morphology of the tubes formed by **1** and the mixture of **1** and **2**. These samples differ from the control Nile red dry sample which forms needle-like crystal structures (Figure S4, Supporting Information).

**ADVANCED
SCIENCE NEWS**
www.advancedsciencenews.com

**ADVANCED
MATERIALS**
www.advmat.de

Reversible *trans*-to-*cis* isomerization of the incorporated azobenzenes in **1** and **2** occurs upon irradiation with UV light (λ = 365 nm), followed by slow relaxation in dark that can also be accelerated by irradiation with visible light. Compound **2** in monomeric state exhibits analogous photoswitching behavior as compound **1**, as observed by UV–vis absorption spectroscopy (10^{-5} M) in acetonitrile (Figure S5, Supporting Information). No significant photodegradation was observed within the timescale of the experiment. In water, supramolecular tubes composed of pure **1** break into shorter segments upon irradiation.[21] This process can be monitored using CD spectroscopy, whereby the pronounced CD signal of compound **1** decreases after irradiation. The identical behavior was observed for the tubes formed by the **1**–**2** mixture with 2% of **2** (Figure 2c). Upon irradiation of 100×10^{-6} M solution of **1**–**2** tubes (50:1) for 45 min, the CD signal decreases by 50% and levels off indicating that the population of the azobenzenes has reached the photostationary state (Figure 2c).

A spectroscopic investigation was conducted to unequivocally confirm incorporation of **2** within the tubular architecture formed by **1**. First, CD spectroscopy was used to assess dynamic exchanges between **2** and **1** in their monomeric form and their self-assembled state in solution. Equimolar proportions of **1** and **2** were used to circumvent problems with the detection limits. Due to the slow dynamic exchange of molecules in self-assembled tubular structures in pure water, the incorporation of **2** into the preformed tubes composed of **1** was studied in 5% MeCN/water mixture, where the dynamic exchanges take place more rapidly.[21] The solution of compound **1** shows evident CD signal, while for compound **2**, no signal is observed. The incorporation of molecules **2** into the tubes is expected to be accompanied by a modification of the degree of helicity due to the dilution of compound **1** within the tubular structure, resulting in a decrease of the CD signal. This effect was monitored in time for three different samples with the same 5×10^{-6} M concentration of **1**: a control experiment, i.e., the solution of **1** (sample I), solution of **2** and **1** mixed in 1:1 ratio prior to the formation of the self-assembled structures (sample II), and the sample prepared by mixing of preassembled 10×10^{-6} M solutions of **1** and **2** in 1:1 volume ratio (sample III). The evolution of the CD signal was followed subsequently (Figure 2d,e).

The shape of the CD spectra was preserved throughout the experiments, which indicates that the specific tubular architecture does not alter significantly (Figure 2d). The CD intensities of the control sample I and mixed solution sample II (Figure 2e) remain steady during the measurement, with the intensity value of sample II being half that of the control sample I despite the same concentration of **1**. This suggests that molecules **2** coassemble with **1**, thus reducing the overall expression of helicity in these chiral tubes. Moreover, the steady intensity of the CD signal of sample II indicates that the exchanges of **2** and **1** between the monomeric state and the assembled state are similar, i.e., there is no propensity for the individual building blocks to form separate structures. In sample III, the initial CD intensity was close to that of sample I, which relates to the equal concentration of **1** in both samples. The initial CD intensity originates from the pure **1** assembled into chiral tubes since the aggregates of **2** display no CD signal. The gradual decrease of the CD intensity in sample III (about 25% within 16 h) suggests

that the expression of chirality deteriorates over time due to the mutual exchanges of **1** and **2** within the self-assembled structures. This is consistent with the CD intensity of sample II displaying a lower CD intensity than that of sample I. This analysis of the CD spectra confirms that **2** successfully incorporates into the chiral tubes in 5% MeCN/water, forming coassembled tubes with a weaker expression of chirality than tubes of **1** alone.

2.3. Formation of Supramolecular Networks by Biotin–Streptavidin Interaction

Spectroscopic CD analysis confirmed that molecules **1** and **2** can coassemble into tubular structures in equimolar ratio. The interaction of SAv with **2** was used to indirectly detect incorporation of **2** into the tubular architecture of **1** at low molar ratio in water. Upon this interaction, supramolecular SAv-tube networks are formed. Microscale thermophoresis (MST), CLSM, and TEM were used to analyze this interaction. MST utilizes the thermophoretic behavior of a fluorescently labeled binding partner in the analysis of noncovalent interactions,[29] given that the magnitude of thermophoresis, i.e., fluorescence change induced by thermophoretic motion, is sensitive to changes in size, charge, and hydration shell of biomolecules.[30,31]

The thermophoretic behavior of Atto-488 fluorescently labeled SAv (SAv-488) at a constant concentration of 100×10^{-9} M was analyzed in solutions of **1** and of **1**–**2** (50:1 ratio). In the solution of **1** below, the CAC (1×10^{-6} M), the thermophoretic mobility of SAv-488 is constant (**Figure 3**a) and similar to its mobility in pure water (Figure S6, Supporting Information). Above the CAC, the thermophoretic mobility becomes concentration dependent (Figure 3a) due to increase of the viscosity of the solution,[29] resulting from the formation of self-assembled structures.[1]

By contrast, thermophoretic analysis of SAv-488 in the solution of **1**–**2** shows a curve (Figure 3b) with a shape that has been previously reported for multivalently interacting proteins and oligonucleotides.[30,32] Further analysis confirms that this is a consequence of thermophoresis and not of the temperature jump (T-jump), i.e., the fluorescence change induced by sample heating (Figure S7, Supporting Information). This indicates that different molecular species with different thermophoretic properties are formed by binding, i.e., complexes of SAv-488 with tubes of diverse lengths and various stoichiometries. The complex of SAv-488 with all four binding sites presaturated with **2** and subsequently mixed with the solution of **1** (Figure S8, Supporting Information) shows a behavior analogous to unbound SAv-488 (Figure 3a), which confirms that the shape of the curve in **1**–**2** is due to the binding of SAv to **2** incorporated within the tubular structure. Furthermore, upon addition of SAv-488 at higher concentration of **1**–**2** tubes (above 100×10^{-6} M of **1**), excessive aggregation prevented MST measurements, while the tubes formed exclusively by **1** still allowed MST measurements in that concentration range (Figure S9, Supporting Information). Thus, the presence of tubes in the solution above the CAC greatly influences the thermophoretic mobility of SAv-488. Specific interactions between SAv-488 and tubes of **1**–**2** are evident from the different thermophoretic behavior of SAv-488 in the solution of **1**–**2** when compared to a solution of purely **1**.
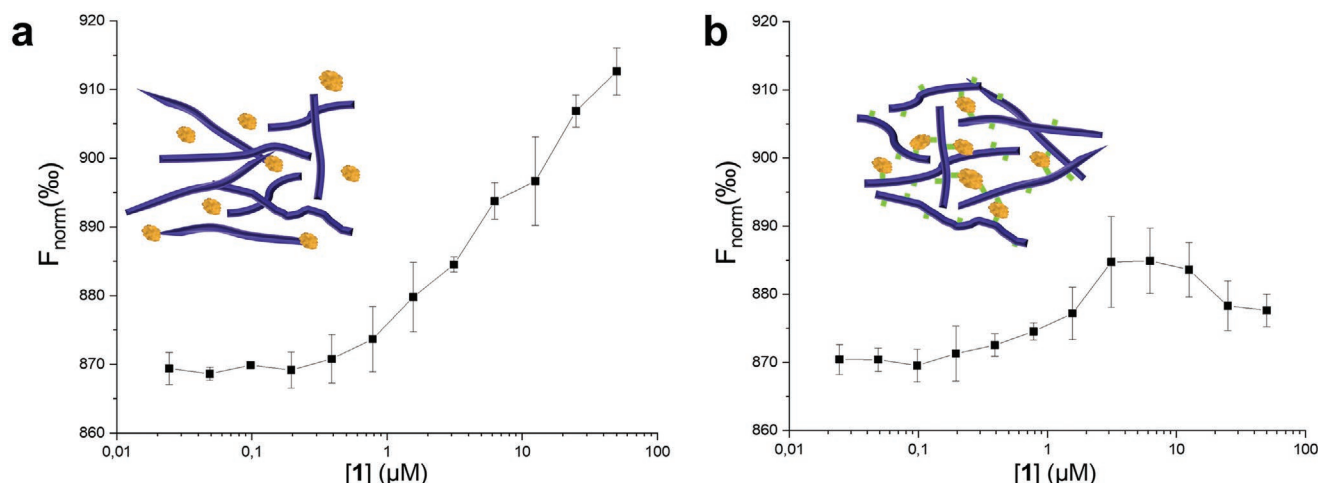
Figure 3. Microscale thermophoresis (MST) measurements. a) Dependence of thermophoretic behavior of SAv-488, represented as a normalized fluorescence (F_{norm}), on the concentration of **1** for the solution of **1**; and b) for the solution of **1–2** (50:1 ratio). [SAv-488] $= 200 \times 10^{-9}$ M, [**1**] $= 100 \times 10^{-6}$ M, dilution 1:1.

As demonstrated by the MST results, the artificial fibrous network can be constructed by using SAv to cross-link biotinylated **1–2** tubes. Such networks were prepared by mixing the solution of fluorescently labeled SAv in various concentrations with the same volume of the solution of preassembled biotinylated tubes at 500×10^{-6} M constant concentration of **1**. The mixed solution was transferred to a compartment of a silicon isolator adhered on a glass slide. The fibrous networks in solution were visualized by CLSM. In addition, TEM was used to analyze the finer structure of the network (**Figure 4**).

A supramolecular network was not observed when SAv was mixed with pure **1** tubes (Figure S10, Supporting Information). Mixing the solution of **1–2** tubes (**1:2** = 50:1) with SAv at different concentrations yields networks with different architectures. At low concentrations of SAv-488 (0.5×10^{-6} M, **2**:SAv = 20), the internal structure of the network is homogeneously distributed (Figure 4a). The cross-section of the fluorescence image shows variation of the fluorescence intensity (Figure 4d). Further, the low contrast observed in differential interference contrast (DIC) image (Figure 4b) indicates small corrugations within the network. At smaller length-scales, the TEM images show aligned elongated tubes that are locally oriented parallel to each other (Figure 4c). When the concentration of SAv-488 increases to 2×10^{-6} M (**2**:SAv = 5), the structure of the network appears larger and/or denser, as indicated by the increased fluorescence intensity within the same volume (Figure 4e). The cross-section of the fluorescence intensity, the DIC image, and the TEM show the formation of porous network formed by elongated tubules (Figure 4e–h). Similar trend of corrugation increase is observed when the density of biotin at the exterior of the tubes is increased. The ratio 10:1 of **1–2** in the tubes yields networks with distinct fibrillar structures with both 5×10^{-6} and 2×10^{-6} M concentrations of SAv (Figure 4i,j and Figure S11a,b (Supporting Information)). The fluorescence intensity cross-section shows multiple well-defined protrusions indicating the formation of bundles. This differs significantly from the systems with lower density of biotin. TEM images show thicker bundles of tubes (Figure 4k) compared to the less

cross-linked networks (Figure 4c,g). Increasing concentration of SAv to 10×10^{-6} or 18×10^{-6} M (**2**:SAv = 2.8 and 5) gives rise to fast uncontrolled cross-linking with insufficient time for the bundles to form (Figure S11c–f, Supporting Information). When the **1:2** ratio is further increased to 5:1, robust gel-like architectures were formed upon addition of SAv (Figure S12, Supporting Information).

In summary, low density of biotin at the exterior of the tubes and low concentration of SAv-488 favor formation of thinner and more homogenous networks, with few local binding sites on the tubes. This allows the tubes to align before cross-linking. Higher density of biotin and higher concentration of SAv (up to the limit of saturation of the four SAv binding sites by biotin) promote faster cross-linking of the tubes and formation of the networks, with random orientations of the tubes imprinted in the resulting networks. At the highest concentrations of the binding partners studied here, the tubes are forced to bundle together in order to maximize the number of connections and these bundles further cross-link together. Based on the flexible concentration range of these SAv–biotin interactions, which exist within the bundles and at their exterior, various network architectures can be established in this system. Finally, the equilibrated networks and tubes appeared stable during the course of the CLSM investigations. This suggest that the incorporation of the biotinylated compound **2** within the tubes is stable and the molecules are not being significantly pulled out by streptavidin[19] as expected, given the slow exchange rates within the system (vide supra).

2.4. Interfacing Non-Cross-Linked Tubes with Supported Lipid Bilayers

In addition to cross-linking between the individual self-assembling tubes, we investigated controlled binding of the non-cross-linked individual supramolecular tubes to functionalized surfaces, i.e., supported lipid bilayers (SLBs). These are common platforms used as plasma membrane mimics in
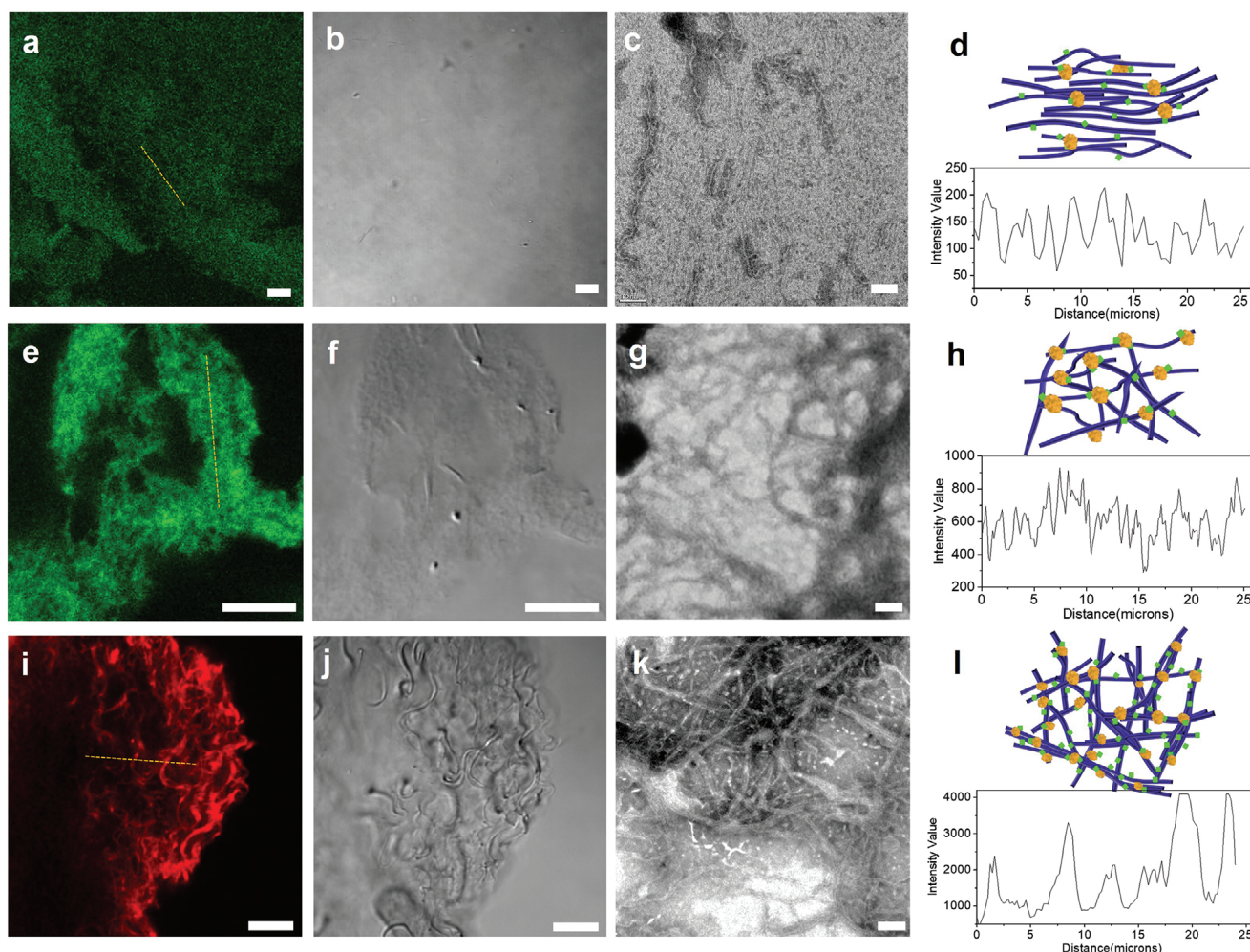
ADVANCED
SCIENCE NEWS
www.advancedsciencenews.com

ADVANCED
MATERIALS
www.advmat.de

Figure 4. CLSM, DIC, and TEM images of the biotinylated tubes–SAv supramolecular network. a–c) Networks formed by **1**–**2** tubes solution (500 × 10^{-6} M, **1:2** = 50:1) mixed with 0.5 × 10^{-6} M SAv Atto-488. e–g) Networks formed by **1**–**2** tubes solution (500 × 10^{-6} M, **1:2** = 50:1) mixed with 2 × 10^{-6} M SAv-488. i–k) Networks formed by mixing of **1**–**2** tubes solution (500 × 10^{-6} M, **1:2** = 10:1) and 5 × 10^{-6} M SAv-565. d,h,l) Illustrations of cross-linked network structure (upper) and cross-sectional profile of fluorescence images (bottom). Networks were obtained by mixing the same volume of SAv Atto-488 and **1**–**2** tubes solutions. Scale bar: (a), (b), (e), (f), (i), (j): 10 μm; (c), (g), (k): 100 nm.

various research fields,[33,34] and are known for their efficient suppression of nonspecific interactions.[35] At the same time, biotin-functionalized SLBs enable the complete coverage of the surface with SAv,[36,37] making them the perfect candidate for surface binding. SLB platforms have already been successfully applied to immobilize collagen fibers[38,39] and cells.[33,40]

The SAv-coated SLBs were constructed in two steps starting from small unilamellar vesicles (SUVs) consisting of 1,2-dioleoyl-*sn*-glycero-3-phosphocholine (DOPC) and 1,2-dioleoyl-*sn*-glycero-3-phosphoethanolamine-*N*-(cap biotinyl) (DOPE-biotin) prepared in a phosphate-buffered saline (PBS) buffer. In contact with the surface of silica as a solid support, SUVs spontaneously rupture resulting in the formation of the SLB with DOPE-biotin at the SLB–water interface.[36] The biotinylated lipid fraction in all experiments was 2%, which assures the complete coverage of the surface with SAv in the subsequent steps.[41,42] SAv binds to such constructed surfaces with two binding sites,[37] leaving the other two binding sites for binding of biotinylated tubes.

The formation of the SLB platform and the subsequent binding of **1**–**2** tubes were monitored in situ with a quartz crystal microbalance method with dissipation monitoring (QCM-D). The adsorption on the QCM sensor is accompanied by the change in frequency (Δ*f*), while the change in energy dissipation (Δ*D*) provides information on the softness of the adsorbed layer. The formation of high-quality SLB was confirmed by frequency shift of Δ*f* = −24 ± 1 Hz (**Figure 5**), which is in agreement with data reported previously.[36,37,42] The binding of SAv to SLB yielded a frequency shift of Δ*f* = −25 ± 1 Hz (Figure 5, black curve), which corresponds to the maximum coverage of the surface with SAv.[42–44] After the formation of the SAv–SLB in PBS buffer, the solvent was switched to Milli-Q water to accommodate the introduction of the water solution of the **1**–**2** tubes. This liquid phase exchange is characterized by the increase in frequency and decrease in dissipation followed by the fast stabilization of the signal. After washing with water for 10 min, the solutions of tubes were introduced into the QCM chambers.
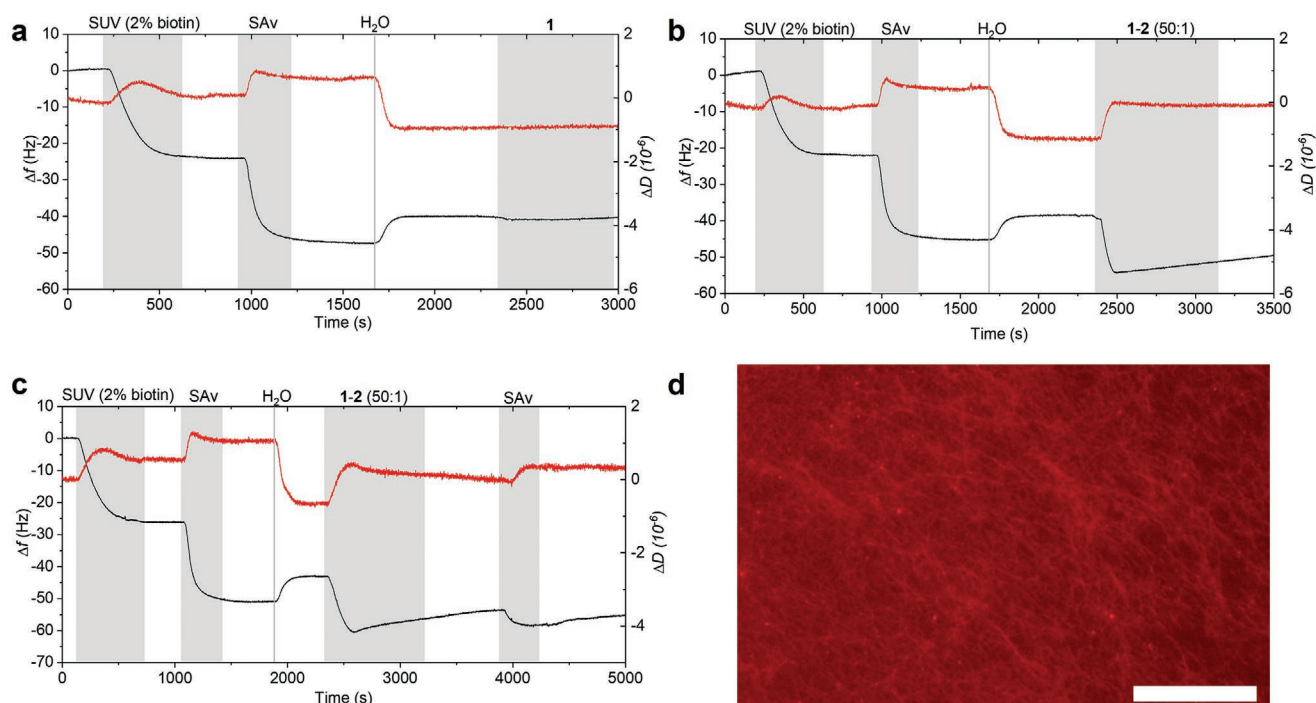
**ADVANCED
SCIENCE NEWS**

www.advancedsciencenews.com

**ADVANCED
MATERIALS**

www.advmat.de

Figure 5. QCM-D measurements of binding of **1–2** tubes to SLB–SAv surface. All samples were prepared with [**1**] = 500×10^{-6} M. Black curves indicate a change in frequency (Δf) over time, red curves indicate a change in energy dissipation (ΔD). a) **1** tubes, b) **1–2** tubes (50:1 ratio), c) **1–2** tubes (50:1 ratio) followed by SAv layer. d) Fluorescent microscopy image of SAv-565 binding on **1–2** tubes attached on the SLB–SAv. Scale bar: 20 μm.

A solution of **1** (500×10^{-6} M) did not yield any frequency shift (Figure 5a), confirming that in the absence of biotins in the structure, the tubes do not bind to the SLB. For the solution of **1–2** with a molar ratio of 300:1 at the concentration of 500×10^{-6} M of **1**, binding was also not observed (Figure S13, Supporting Information). When the proportion of **2** was increased in **1–2** while keeping the same concentration of **1** (50:1, [**1**] = 500×10^{-6} M), clear evidence of binding was observed as a distinct frequency shift (Figure 5b). Furthermore, owing to accessible biotin groups remaining at the outside layer of the **1–2** tubes, the attachment of a next layer of SAv on the tubes layer was accomplished (Figure 5c). Fiber-like patterns observed in fluorescent microscopy images (Figure 5d) confirmed the specific binding of **1–2** tubes to SAv–SLB. Meanwhile, if tube **1** was introduced instead, no obvious structure and fluorescence was detected (Figure S14, Supporting Information) indicating the absence of nonspecific binding, which is consistent with the QCM result (Figure 5a).

Binding was also obtained for a lower concentration of **1** (250×10^{-6} M) in **1–2** while maintaining the same 50:1 molar ratio of the monomers (Figure S15, Supporting Information). Distinct binding was also observed for the solution of **1–2** with the molar ratios of 120:1 and 60:1 (Figure S16, Supporting Information), and at a constant concentration of **2** (1.67×10^{-6} M, with **1:2** = 200×10^{-6}:1.67×10^{-6} and 100×10^{-6}:1.67×10^{-6} M) (Table S1, Supporting Information). This confirmed that the absence of binding in the case of **1–2** with 300:1 molar ratio was not a consequence of low concentration of compound **2** (1.67×10^{-6} M), but was actually a result of the low molar ratio of **2** incorporated in the tubular architecture.

In order to observe the effect of irradiation on subsequent binding of biotinylated tubes on the surface, 500×10^{-6} M solution of **1–2** (50:1) tubes was divided into two samples. One sample was irradiated for 60 min in 2 mm quartz cuvette and the other one was left in dark. The binding of tubes from the irradiated sample to a SLB–SAv platform showed a higher QCM frequency shift than the nonirradiated one (Figure S17, Supporting Information). The irradiated sample also showed a larger dissipation signal. This indicates that smaller segments formed during irradiation cover the modified surface more efficiently than longer tubes.

2.5. Binding of the SAv-Cross-Linked Networks of Tubes on Biotinylated SLB

Following the successful binding of individual supramolecular tubules to SLB, we explored the potential of the SAv-cross-linked networks of tubes to bind to the functionalized SLBs. Given that the number of connecting points is crucial for successful attachment of individual tubes, it was expected that the same would apply for the tubes–SAv network. In order to confirm the binding, QCM was not an appropriate technique due to the lower counts and larger sizes of the network formed in contrast to its use for non-cross-linked tubes discussed in the previous section. Therefore, CLSM was used for sample analysis.

Glass slides for CLSM were coated with biotinylated SLB prepared by fusion of SUVs, comprising of DOPC doped with DOPE-biotin, on a clean bare glass slide. The solution of
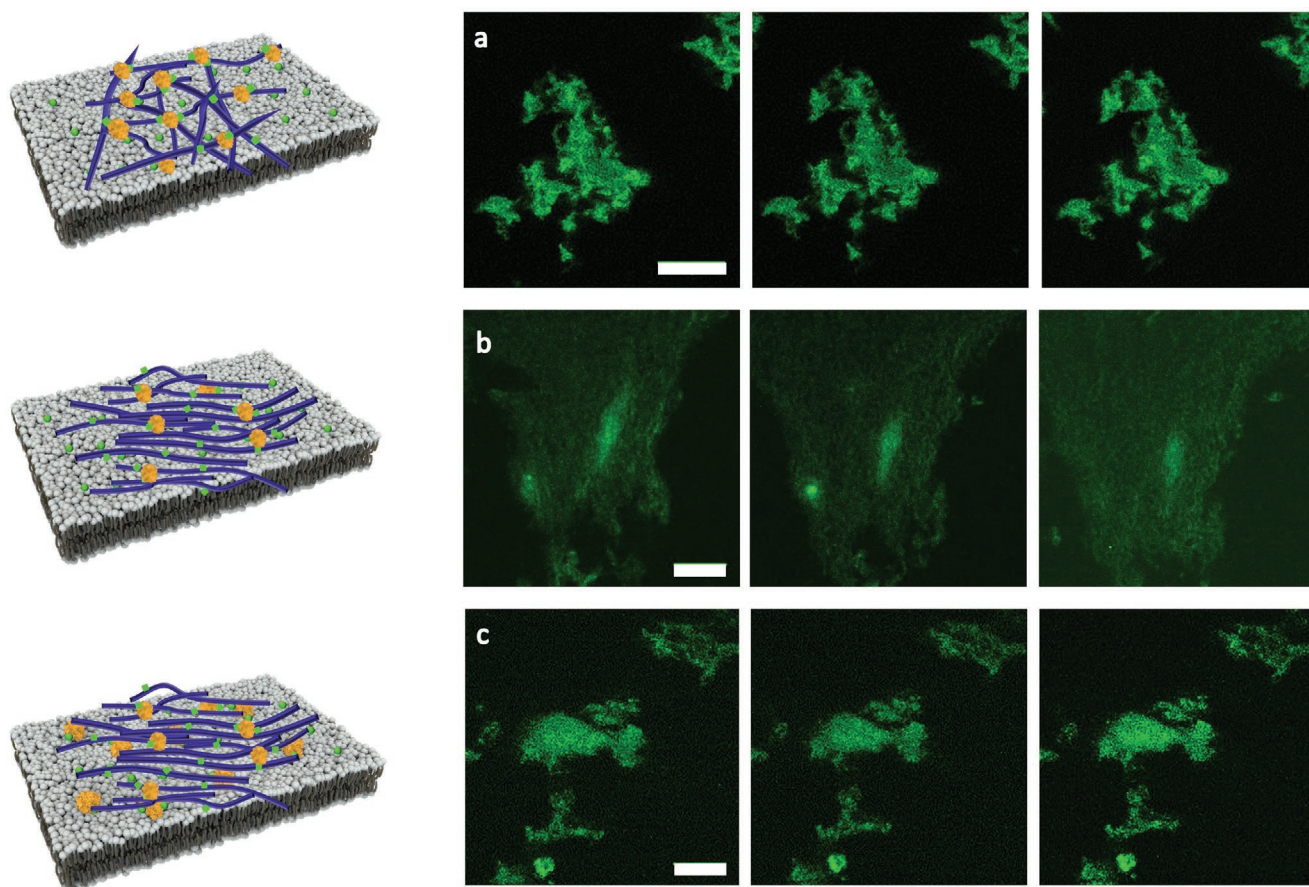
ADVANCED
SCIENCE NEWS
www.advancedsciencenews.com

ADVANCED
MATERIALS
www.advmat.de

Figure 6. Immobilization of SAv-cross-linked tube networks. CLSM time sequence images (image interval = 60 s) of tubes–SAv networks formed with a) 2×10^{-6} M, b) 0.5×10^{-6} M SAvs on biotinylated SLB. c) Tubes–SAv network formed with 0.5×10^{-6} M SAv on SLB–SAv platform. Scale bar: 20 µm.

cross-linked networks, prepared by mixing a solution of **1–2** tubes (500×10^{-6} M, **1:2** = 50) with SAv, was introduced onto biotinylated SLB directly. After the network was added to the biotinylated SLB substrate, further rinsing was applied to remove most of the nonattached, floating network aggregates from the surface. The network formed by adding 2×10^{-6} M solution of SAv to a solution of **1–2** tubes resulted in successful immobilization (**Figure 6**a) due to the binding of unsaturated SAvs, exposed at the outside of the network, to the biotins of the SLB. The **2**:SAv ratio of 5:1 ensured effective cross-linking between the tubes within the network, and minimized the possibility of the presence of free SAv in the solution. When biotin is not present on the SLB surface, the bundled networks drifted slowly away from the investigated area which shows the importance of the biotin–SAv binding for effective immobilization of the networks (Figure S18, Supporting Information).

Lowering the amount of SAv (0.5×10^{-6} M, **2**:SAv = 20) leads to the formation of a tenuous network drifting on the biotinylated SLBs (Figure 6b), indicating that the density of SAv at the outer part of the network is insufficient to provide enough connecting points essential for binding. However, when SAv is first bound to the biotinylated SLB (SLB–SAv platform), followed by the addition of the tubes–SAv network, the immobilization is effective owing to the sufficient number of biotin linkers available at the network exterior (Figure 6c). This implies

that effective binding only occurs when complementary binding sites are available at the networks and the SLB substrates.

Finally, the influence of irradiation on the SAv-cross-linked tube networks was investigated by CLSM in combination with CD measurements. The samples were prepared by mixing the same volume of 2×10^{-6} M Atto-565 fluorescently labeled SAv (SAv-565) solution and of biotinylated tubes solution (500×10^{-6} M, **1:2** = 50). The solution was drop casted into a 2 mm thick compartment of a silicone isolator adhered to a bare glass slide and covered with a glass coverslip. The chamber was then irradiated with UV light (λ = 365 nm) for 5 min. During the UV irradiation, the network undergoes structural changes including apparent shrinking (**Figure 7**). The cross-sectional profiles of the fluorescence images show that the structure becomes narrower, indicating the formation of a tighter network. After the irradiation stopped, 50 µL of the sample was diluted with water to 200 µL and CD measurements were performed. These spectra were compared with nonirradiated solution diluted in the same way. The significant decrease in the CD signal of the irradiated samples (Figure S19, Supporting Information) demonstrates decrease in supramolecular chirality of the system attributed to breaking and partial disassembly of the tubes.[21] Moreover, *trans*-to-*cis* transitions of the azobenzene unit, which are rare within a well ordered supramolecular tube, are more probable in the immediate vicinity of an existing
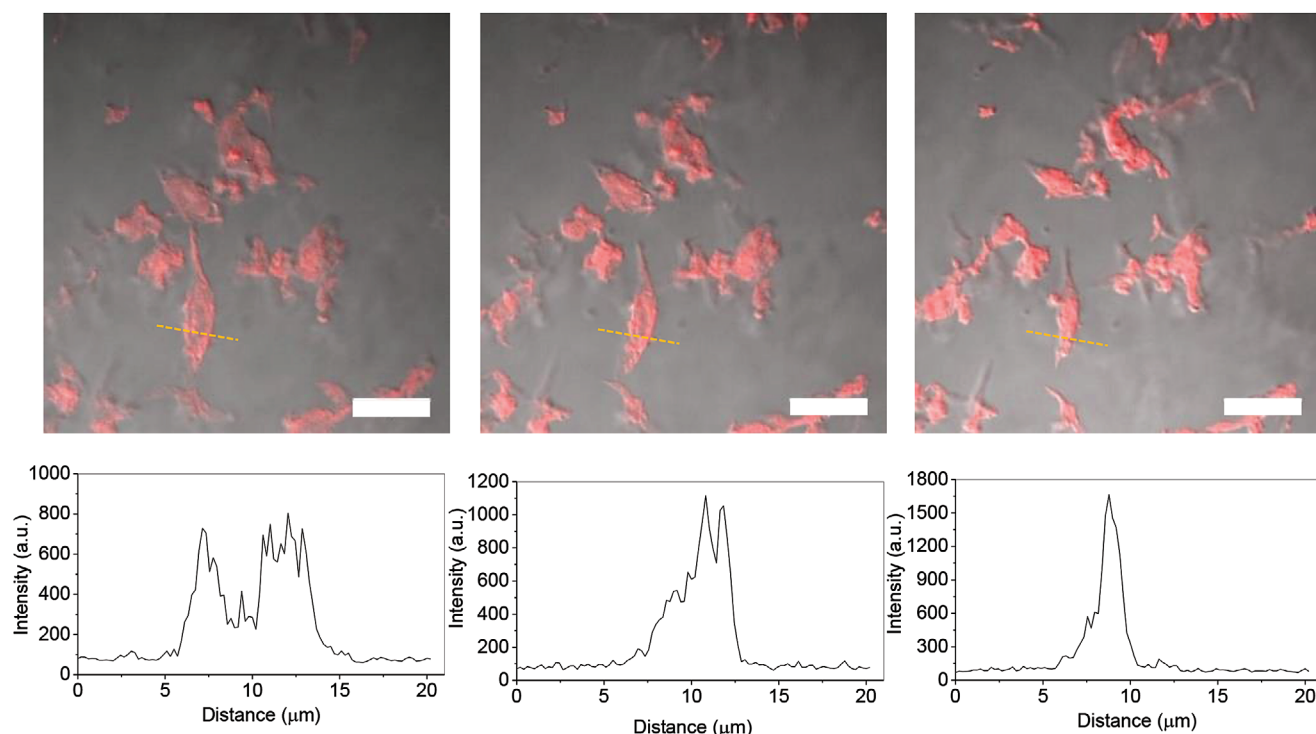
**ADVANCED
SCIENCE NEWS**

www.advancedsciencenews.com

**ADVANCED
MATERIALS**

www.advmat.de

Figure 7. The influence of irradiation on the cross-linked tubes–SAv networks. CLSM time sequence images (merged fluorescence and DIC) of the network formed by **1**–**2** tubes (500×10^{-6} M, **1:2** = 50:1) and 2×10^{-6} M SAv-565 under irradiation with UV light ($\lambda = 365$ nm) for 5 min. Images were taken at (left to right) 0, 2.5, 5 min. Cross-sectional profiles of the fluorescence images are shown below. Scale bar: 20 μm.

defect.[45] As a result, a "brittle-like" tube breakage leads to the formation of shorter segments. When supramolecular tubes are free in the solution, they can move apart. Here, however, the SAv–biotin interaction between the tubes limits their movement after the breaking. Our results suggest that shorter tubes' segments allow the rearrangement of the network by binding to accessible SAv binding sites that were previously sterically hindered. Thus, shrinking takes place and more condense networks are formed with smaller pores within the supramolecular network due to inhomogeneous distribution of binding sites.

supramolecular tubes and their SAv-cross-linked networks to demonstrate a tunable affinity to biotinylated SLBs. Such hierarchically ordered self-assembled architectures interacting with the lipid bilayers approach the complexity of interactions between cells and extracellular matrix. Understanding these interactions on simplified model system enables the exploration of otherwise complex processes, while the strategy of building such a hybrid hierarchical supramolecular network can serve as a model for other biomimetic systems and tissue engineering studies.

3. Conclusion

The current rapid development of biomimetic materials urges a focus toward model systems that enable an understanding of the mechanism of the interaction of artificial materials with cells, i.e., cell membranes. In this study, we have explored and demonstrated a strategy for controlled cross-linking of self-assembled tubes and their binding to SLBs either on the level of individual tubes or as cross-linked networks.

Our strategy consists of the coassembly of small organic monomers into tubular architectures decorated with a controlled density of biotin, which are able to bind to an external multivalent binding partner in the form of dissolved four-valent SAv. Depending on the concentration and the ratio between all three components, i.e., monomer, biotinylated monomer, and SAv, different hierarchical structures were formed, allowing us to demonstrate the formation of multitude of network architectures using the same building blocks. We then used our

4. Experimental Section

General: All chemicals for synthesis of **1** and **2** were purchased from Sigma-Aldrich and used without further purification, unless stated otherwise. DOPC and DOPE-biotin sodium salt were purchased from Avanti Polar Lipids. SAv (salt-free, lyophilized powder), SAv-488, and SAv-565 were purchased from Sigma-Aldrich. Compound **1** was prepared according to the previously reported procedure.[21] Detailed synthetic procedure for the preparation of compound **2** is given in the Supporting Information.

Preparation of Solutions of Supramolecular Tubes: The solutions of **1** and multicomponent **1**–**2** samples in varying ratios were prepared from concentrated stock solutions of **1** and **2** in acetonitrile (ACN). The required volumes of solutions **1** and **2** in ACN were mixed and the solvent was evaporated under the nitrogen flow. Resulting residue was rehydrated in Milli-Q water with the final concentrations in micromolar range and left overnight before proceeding with the experiments.

Preparation of Small Unilamellar Vesicles: The SLB was prepared using the vesicle fusion method. SUVs were prepared at first using the hydration and extrusion method.[46]

2105926 (9 of 11)

ADVANCED
SCIENCE NEWS

www.advancedsciencenews.com

ADVANCED
MATERIALS

www.advmat.de

Briefly, a lipid mixture of 98.0 mol% DOPC and 2.0 mol% DOPE-biotin was prepared by mixing a stock solution of DOPC (10 mg mL^{-1}) and DOPE-biotin (0.1 mg mL^{-1}) in chloroform. This lipid mixture was further injected into a glass vial and evaporated under a gentle flow of nitrogen gas until lipid films formed on the wall. Then, the vial was put into a vacuum desiccator for at least 1 h to remove the chloroform completely. Afterward, 1 mL of Milli-Q water was injected, and the vial was shaken until all lipids were hydrated and dissolved from the wall of the vial. The opaque aqueous solution was then extruded 11 times with a Mini-Extruder kit (Avanti Polar Lipids), equipped with a polycarbonate membrane of 100 nm pores (Whatman) to form SUVs. This SUV solution was stored in the refrigerator and used within 2 weeks.

UV–Visible and CD Spectroscopy: UV–visible spectra were recorded at room temperature with a Perkin Elmer Lambda 850 UV–visible spectrometer. CD spectra were recorded with a Jasco J1500 spectrometer. Samples of lower concentrations (<10 × 10^{-6} M) were measured in 1 cm quartz cuvettes, while the samples of higher concentrations were measured in 1 mm quartz cuvettes. The solutions were prepared at least 18 h before the measurements, except for the dynamic exchange experiments in acetonitrile, for which the samples were prepared freshly prior to the measurements.

TEM: The samples were prepared by drop casting solutions of biotinylated tubes–SAv supramolecular network solution on carbon grids (Formvar/Carbon 200 mesh, Copper). Prior to measurements, the samples were stained with 2% phosphotungstic acid. TEM images were recorded using a Philips CM300ST – FEG microscope. The Image J 1.46 software was used to analyze the TEM images. Manual analysis led to determination of the diameter of the tubes.

MST Measurement: MST measurements were performed using the Monolith NT.115 (NanoTemper Technologies GmbH, Germany). Standard treated capillary tubes were used (NanoTemper, LLC, Munich, Germany) for measuring, and all data sets were collected at ambient temperature, i.e., ≈22 °C. Concentration series of **1** or **1–2** were prepared using a 1:1 serial dilution of the sample into Milli-Q water, with the top [**1**] = 100 × 10^{-6} M; 12 samples of 10 µL were thus prepared, ranging in concentration from 100 × 10^{-6} to 49 × 10^{-9} M. The association was initiated by the addition of 10 µL of 200 × 10^{-9} M SAv-488 solution to each of the 12 samples, resulting in the final SAv-488 concentration of 100 × 10^{-9} M and also halving all of the concentrations of **1**. The obtained mixed samples were loaded into capillary tubes and inserted into the apparatus for the data acquisition. The pre-MST period was 5 s, the MST-acquisition period was 30 s, and the post-MST period was 5 s. The light emitting diode (LED) power (i.e., the power supplied to the excitation LED) was 70%. Each experiment was conducted with three MST powers (i.e., the power supplied to the IR laser) – 20%, 40%, and 80%. For the analysis, MST power of 40% was used. Analysis was conducted in (thermophoresis + T-jump) mode unless stated otherwise.

Preparation of the SLB and Immobilization of Supramolecular Tubes and Networks for Fluorescent Microscopy: For fluorescent microscopy, CLSM (Nikon A1) equipped with 488 nm laser, a 525/50 nm emission filter, and DIC accessories were used to observe biotinylated networks and the immobilization. Fluorescence microscopy (Plympus, BX53) was used to observe dry tubes and immobilization of biotinylated tubes. Silicone isolators used for fluorescent microscopy measurements were purchased from Electron Microscopy Science.

Herein, the SLB was deposited on a glass slide with a silicone chamber. Before the formation of the SLB, 2 M sodium hydroxide solution was added to a glass substrate for 1 h to increase the hydrophilicity of the glass surface. Afterward, the chambers were rinsed with Milli-Q water and immersed in 0.1 M PBS buffer (0.1 M sodium dihydrogen phosphate and 0.15 M sodium chloride, pH 7.4). A SUV solution (volume ratio of SUV solution to PBS buffer solution is 1:9) was added and incubated for 30 min at room temperature. A defect-free SLB was formed by the rupture of SUVs onto the hydrophilic glass substrate. Excess lipids were removed from the chamber by rinsing it with Milli-Q water at least 3 times. The biotinylated SLBs were incubated with 50 µg mL^{-1} SAv solution for 30 min and rinsed with Milli Q water 3 times. Following that, the sample was incubated with the solution of biotinylated tubes for 30 min. After 30 min, the samples were gently rinsed 3 times and the chamber was capped with a covered slide and sealed with a nail polish.

QCM-D Measurements: QCM-D measurements were performed using a Qsense Analyzer (Biolin Scientific). Measurements were performed at 22 °C and operated with four parallel flow chambers using two peristaltic pumps (Ismatec) with a flow rate of 50 µL min^{-1}. Throughout this work, the fifth overtone was used for the normalized frequency (Δf_5) and dissipation (ΔD_5). SiO$_2$-coated sensors (QSX303, Biolin Scientific) were used. Before measurement, SiO$_2$ chips were sonicated in 2 wt% sodium dodecyl sulfate solution and Milli-Q water successively. After drying under N$_2$ flow, activation was performed using UV/ozone treatment (UV/ozone ProCleaner, BioForce Nanosciences) for 20 min. During the addition of the solutions of the tubes, these solutions were recycled after they started flowing out of the outward tubing.

For the SLB preparation during the QCM-D measurements, SUVs were dissolved in 0.1 M PBS buffer (0.1 M sodium dihydrogen phosphate and 0.15 M sodium chloride, pH 7.4) with SUV and PBS solution volume ratio 1:9. SAv was dissolved in Milli-Q water at a concentration of 50 µg mL^{-1}. SLB formation was achieved by flowing SUV solution on an activated surface in the closed flowing chamber. After the SLB formation, care was taken to keep the chip wet during and in between all subsequent steps.

Supporting Information

Supporting Information is available from the Wiley Online Library or from the author.

Conflict of Interest

The authors declare no conflict of interest.

Data Availability Statement

The data that support the findings of this study are available from the corresponding author upon reasonable request.

**ADVANCED
SCIENCE NEWS**

www.advancedsciencenews.com

**ADVANCED
MATERIALS**

www.advmat.de

[1] S. Seiffert, J. Sprakel, *Chem. Soc. Rev.* **2012**, *41*, 909.

[2] R. Picu, *Soft Matter* **2011**, *7*, 6768.

[3] D. H. Wachsstock, W. H. Schwarz, T. D. Pollard, *Biophys. J.* **1994**, *66*, 801.

[4] S. Bodakuntla, A. S. Jijumon, C. Villablanca, C. Gonzalez-Billault, C. Janke, *Trends Cell Biol.* **2019**, *29*, 804.

[5] E. W. Flitney, E. R. Kuczmarski, S. A. Adam, R. D. Goldman, *FASEB J.* **2009**, *23*, 2110.

[6] M. Bezanilla, A. S. Gladfelter, D. R. Kovar, W. L. Lee, *J. Cell Biol.* **2015**, *209*, 329.

[7] C. D. Reyes, T. A. Petrie, A. J. García, *J. Cell. Physiol.* **2008**, *217*, 450.

[8] O. Goor, S. I. S. Hendrikse, P. Y. W. Dankers, E. W. Meijer, *Chem. Soc. Rev.* **2017**, *46*, 6621.

[9] E. Ruoslahti, M. D. Pierschbacher, *Science* **1987**, *238*, 491.

[10] W. E. Hennink, C. F. van Nostrum, *Adv. Drug Delivery Rev.* **2012**, *64*, 223.

[11] K. Vanherck, G. Koeckelberghs, I. F. J. Vankelecom, *Prog. Polym. Sci.* **2013**, *38*, 874.

[12] K. Schuh, O. Prucker, J. Ruhe, *Macromolecules* **2008**, *41*, 9284.

[13] M. Pérez-Perrino, R. Navarro, O. Prucker, J. Rühe, *Macromolecules* **2014**, *47*, 2695.

[14] S. Sim, D. Miyajima, T. Niwa, H. Taguchi, T. Aida, *J. Am. Chem. Soc.* **2015**, *137*, 4658.

[15] M. Fernández-Castaño Romera, X. Lou, J. Schill, G. ter Huurne, P.-P. K. Fransen, I. K. Voets, C. Storm, R. P. Sijbesma, *J. Am. Chem. Soc.* **2018**, *140*, 17547.

[16] T. Aida, E. W. Meijer, S. I. Stupp, *Science* **2012**, *335*, 813.

[17] R. Freeman, M. Han, Z. Álvarez, J. A. Lewis, J. R. Wester, N. Stephanopoulos, M. T. McClendon, C. Lynsky, J. M. Godbe, H. Sangji, E. Luijten, S. I. Stupp, *Science* **2018**, *362*, 808.

[18] S. P. W. Wijnands, W. Engelen, R. P. M. Lafleur, E. W. Meijer, M. Merkx, *Nat. Commun.* **2018**, *9*, 65.

[19] D. Amado Torres, M. Garzoni, A. V. Subrahmanyam, G. M. Pavan, S. Thayumanavan, *J. Am. Chem. Soc.* **2014**, *136*, 5385.

[20] G. Morgese, B. F. M. de Waal, S. Varela-Aramburu, A. R. A. Palmans, L. Albertazzi, E. W. Meijer, *Angew. Chem., Int. Ed. Engl.* **2020**, *132*, 17382.

[21] J. W. Fredy, A. Mendez-Ardoy, S. Kwangmettatam, D. Bochicchio, B. Matt, M. C. A. Stuart, J. Huskens, N. Katsonis, G. M. Pavan, T. Kudernac, *Proc. Natl. Acad. Sci. USA* **2017**, *114*, 11850.

[22] Z. Huang, S.-K. Kang, M. Banno, T. Yamaguchi, D. Lee, C. Seok, E. Yashima, M. Lee, *Science* **2012**, *337*, 1521.

[23] O. H. Laitinen, V. P. Hytonen, H. R. Nordlund, M. S. Kulomaa, *Cell. Mol. Life Sci.* **2006**, *63*, 2992.

[24] M. O. Guler, S. Soukasene, J. F. Hulvat, S. I. Stupp, *Nano Lett.* **2005**, *5*, 249.

[25] K. Petkau-Milroy, M. H. Sonntag, A. Colditz, L. Brunsveld, *Int. J. Mol. Sci.* **2013**, *14*, 21189.

[26] D. Kim, A. E. Herr, *Biomicrofluidics* **2013**, *7*, 041501.

[27] M. Gonzalez, L. A. Bagatolli, I. Echabe, J. L. R. Arrondo, C. E. Argarana, C. R. Cantor, G. D. Fidelio, *J. Biol. Chem.* **1997**, *272*, 11288.

[28] M. Gonzalez, C. E. Argarana, G. D. Fidelio, *Biomol. Eng.* **1999**, *16*, 67.

[29] C. J. Wienken, P. Baaske, U. Rothbauer, D. Braun, S. Duhr, *Nat. Commun.* **2010**, *1*, 100.

[30] M. Jerabek-Willemsen, T. André, R. Wanner, H. M. Roth, S. Duhr, P. Baaske, D. Breitsprecher, *J. Mol. Struct.* **2014**, *1077*, 101.

[31] M. Asmari, R. Ratih, H. A. Alhazmi, S. El Deeb, *Methods* **2018**, *146*, 107.

[32] T. H. Scheuermann, S. B. Padrick, K. H. Gardner, C. A. Brautigam, *Anal. Biochem.* **2016**, *496*, 79.

[33] R. Glazier, K. Salaita, *Biochim. Biophys. Acta, Biomembr.* **2017**, *1859*, 1465.

[34] G. J. Hardy, R. Nayak, S. Zauscher, *Curr. Opin. Colloid Interface Sci.* **2013**, *18*, 448.

[35] J. K. van Weerd, M. Jonkheijm, *Adv. Healthcare Mater.* **2015**, *4*, 2743.

[36] T. K. Lind, M. Cárdenas, *Biointerphases* **2016**, *11*, 020801.

[37] G. V. Dubacheva, C. Araya-Callis, A. G. Volbeda, M. Fairhead, J. Codee, M. Howarth, R. P. Richter, *J. Am. Chem. Soc.* **2017**, *139*, 4157.

[38] S. Vafaei, S. R. Tabaei, N. J. Cho, *ACS Omega* **2017**, *2*, 2395.

[39] C.-J. Huang, N.-J. C., C. W. Frank, P.-Y. Tseng, C. W. Frank, Y.-C. Chang, *Biomacromolecules* **2010**, *11*, 1231.

[40] M. Bennett, M. Cantini, J. Reboud, J. M. Cooper, P. Roca-Cusachs, M. Salmeron-Sanchez, *Proc. Natl. Acad. Sci. USA* **2018**, *115*, 1192.

[41] E. Nileback, L. Feuz, H. Uddenberg, R. Valiokas, S. Svedhem, *Biosens. Bioelectron.* **2011**, *28*, 407.

[42] D. Di Iorio, M. L. Verheijden, E. van der Vries, P. Jonkheijm, J. Huskens, *ACS Nano* **2019**, *13*, 3413.

[43] F. Hook, A. Ray, B. Norden, B. Kasemo, *Langmuir* **2001**, *17*, 8305.

[44] C. Larsson, M. Rodahl, F. Hook, *Anal. Chem.* **2003**, *75*, 5080.

[45] D. Bochicchio, S. Kwangmettatam, T. Kudernac, G. M. Pavan, *ACS Nano* **2019**, *13*, 4322.

[46] R. C. MacDonald, R. I. MacDonald, B. P. M. Menco, K. Takeshita, N. K. Subbarao, L.-r. Hu, *Biochim. Biophys. Acta, Biomembr.* **1991**, *1061*, 297.

2105926 (11 of 11)